

M. Alfredsson · J. P. Brodholt · D. P. Dobson
A. R. Oganov · C. R. A. Catlow · S. C. Parker
G. D. Price

Crystal morphology and surface structures of orthorhombic MgSiO₃ perovskite

Received: 9 December 2003 / Accepted: 1 September 2004 / Published online: 13 January 2005
© Springer-Verlag 2005

Abstract Orthorhombic MgSiO₃ perovskite is thought to be the most abundant mineral in the mantle of the Earth. Its bulk properties have been widely studied, but many geophysical and rheological processes are also likely to depend upon its surface and grain boundary properties. As a first step towards modelling these geophysical properties, we present here an investigation of the structures and energetics of the surfaces of MgSiO₃-perovskite, employing both shell-model atomistic effective-potential simulations, and density-functional-theory (DFT) calculations. Our shell-model calculations predict the {001} surfaces to be the energetically most stable surfaces: the calculated value of the surface energy being 2.2 J/m² for the MgO-terminated surface, which is favoured over the SiO₂-terminated surface (2.7 J/m²). Also for the polar surfaces {111}, {101} and {011} the MgO-terminated surfaces are energetically more stable than the Si-terminated surfaces. In addition we report the predicted morphology of the MgSiO₃ perovskite structure, which is dominated by the energetically most stable {001} and {110} surfaces, and which appears to agree well with the shape of grown single crystals.

Keywords Perovskite · Morphology · Surface structures · Grain boundary · Mantle · Modelling

Introduction

Perovskite structured MgSiO₃ is believed to comprise 70% of the lower mantle, and it is thus the most abundant mineral in the Earth. Numerous experimental investigations on the MgSiO₃ structure have been reported, the majority of which have focussed on its bulk properties (e.g. Fiquet et al. 2000; Fiquet et al. 1998; D. Yamazaki et al. 2000; Bolfan-Casanova et al. 2002; Andraut et al. 2001; Chen et al. 2002; Fei and Wang 2000). However, experimental studies at representative mantle pressures and temperatures are difficult, and so theoretical methods have also been of great value in predicting some of the properties of MgSiO₃ under the pressure and temperature conditions to be found in the mantle (e.g. Oganov et al. 2000; Oganov et al. 2001; Parlinski and Kawazoe 2000; Karki et al. 2001; Karki et al. 2000; Stixrude et al. 1998; Stixrude and Cohen 1993; Marton and Cohen 2002; Matsui 2000). Despite these high quality, first principles and inter-atomic potential calculations on the bulk behaviour of MgSiO₃ perovskite, no detailed modelling of its surfaces has so far been reported. The aim of the current investigation is to determine the geometrical structures and energies of the surfaces of MgSiO₃ perovskite. Surface calculations are often highly demanding of computer resources, so we have used both high level ab initio calculations, as well as the more computationally efficient inter-atomic potential based models. These potential models have previously been shown to give a good description of the bulk structure of the MgSiO₃ perovskite (Wright and Price 1993; Wright and Price 1989; Wall and Price 1989; Price et al. 1989; Wall et al. 1986; Watson et al. 2000), and in this study we have investigated whether they can also be used to model perovskite surfaces, by comparing

M. Alfredsson (✉) · C. R. A. Catlow
Davy Faraday Research Laboratory,
The Royal Institution of Great Britain,
21 Albemarle Street, London, W1S 4BS, UK
E-mail: m.alfredsson@ucl.ac.uk

M. Alfredsson · J. P. Brodholt · D. P. Dobson · A. R. Oganov
G. D. Price
Department of Earth Sciences,
University College London, Gower Street,
London, WC1E 6BT, UK

A. R. Oganov
Laboratory of Crystallography, Department of Materials,
ETH Zurich, CH-8092 Zurich, Switzerland

S. C. Parker
Department of Chemistry, Bath University,
Bath, BA2 7AY, UK

the results that they give with the more accurate *ab initio* simulations.

Our interest in surface structures is driven by the eventual need to understand the rheological properties of the lower mantle, which one presumes depend upon the behaviour of polycrystalline aggregates of MgSiO₃-rich perovskite, their grain boundary processes, and possibly on their crystal morphology. Furthermore, because of the reactivity of surfaces with respect to small molecules (e.g. H₂O), ionic impurities (such as Ca²⁺), and other trace elements present in the mantle, it is vital to understand which surface structures (e.g. non-polar (less reactive) or polar (reactive) surfaces) are favoured in MgSiO₃ perovskite. The work presented here lays the foundations for further modelling of the rheology and bulk properties of perovskite rock, which will critically depend upon grain boundary and related surface processes. In the current investigation we discuss both non-polar surfaces as well as polar surfaces. However, owing to large surface reconstructions, the latter type of surfaces are often less stable than the non-polar surfaces, causing special computational problems. Consequently, less information on these types of surfaces is reported.

In this paper we briefly summarize the salient aspects of the perovskite structure, and critically discuss the *ab initio* and empirical methods that we use, with particular reference to the problems of modelling surfaces. In section 4, we present the detailed results of our simulation, and end by comparing our predicted equilibrium morphology for MgSiO₃ perovskite with that of crystals recently synthesized in a multi-anvil high pressure cell.

Geometrical structure

MgSiO₃ perovskite crystallises with an orthorhombic structure—space group *Pbnm* (Ross and Hazen 1989), with the tetravalent cations (Si) in an octahedral environment (see Fig. 1), forming a linked network of corner sharing SiO₆ octahedra, with the divalent cations (Mg) occupying a distorted 12-fold coordinated site. As can be seen from Fig. 1, the SiO₆ octahedra tilt while the Mg²⁺-ions are in a lower symmetric site within the SiO₆-cages.

There is no experimental data on the surface structures of MgSiO₃, so we compare our results with the information that is available on BaTiO₃, PbTiO₃ and SrTiO₃ perovskites. These phases have been well studied because of their importance as ferroelectric materials. The relationships between the crystallographic space groups of the latter structures and the orthorhombic structure of MgSiO₃ are well known, but for clarity are highlighted here. The orthorhombic structures of ATiO₃ (A = Ba, Pb and Sr) can be derived from their cubic structure, which belongs to space group *Pm.3m* (Wykoff 1965; see Fig. 2a), by a distortion first in the $\langle 001 \rangle$ and secondly in the $\langle 110 \rangle$ directions. The space group of

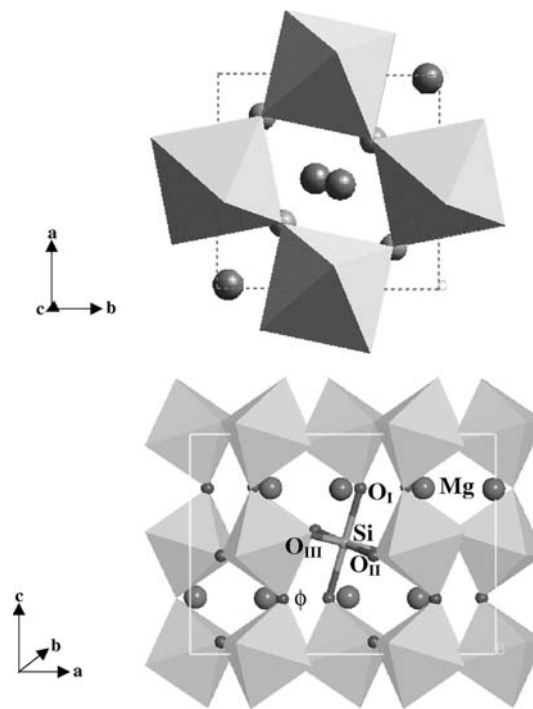


Fig. 1 a View along the *c*-axis and b along the *b*-axis of the *Pbnm* perovskite structure of MgSiO₃. SiO₆-octahedra marked in light grey, Mg-ions and O-ions are marked as larger and smaller dark grey balls

the orthorhombic structure of the ferroelectric materials (BaTiO₃, PbTiO₃ and SrTiO₃) is, however, different from the *Pbnm* structure for MgSiO₃, as they crystallise in the *Amm2* structure (Wykoff 1965; see Fig. 2b and c). From Fig. 1 we can see that the network of BO₆ (B = Si) octahedra are running along the *c*-axis in the *Pbnm* structure, while in the *Amm2* structure the BO₆ (B = Ti) network is linked along the *a*-axis (see Figs. 2b and c). The surface indices for the two structures are, therefore, different, and as shown in Table 1 the {001} surface of the *Pbnm* structure corresponds to the {100} surface of the *Amm2* structure. In Table 1 we present the Miller indices for the *Pbnm*, *Amm2* and *Pm.3m* structures.

Methods

Computational details

In the current study we employed both density-functional theory (DFT) plane wave calculations and static lattice simulations using effective pair potentials to model the surfaces of MgSiO₃. The computational details for the two methods are given separately below. The main reason for using the computer-intensive *ab initio* plane wave calculations was to check the reliability of the inter-atomic potentials employed in the work, and to obtain a control on how truly transferable they are to the study of surfaces and grain boundaries.

Fig. 2 a The $Pm\bar{3}m$ structure of the cubic perovskite structure, **b** view along the a -axis of and **c** along the b -axis of the orthorhombic $Amm2$ perovskite structure of $ATiO_3$, where A corresponds to Ba, Pb or Sr. TiO_6 -octahedra marked in light grey, A-ions as larger dark grey balls, and O-ions are marked as small dark grey balls

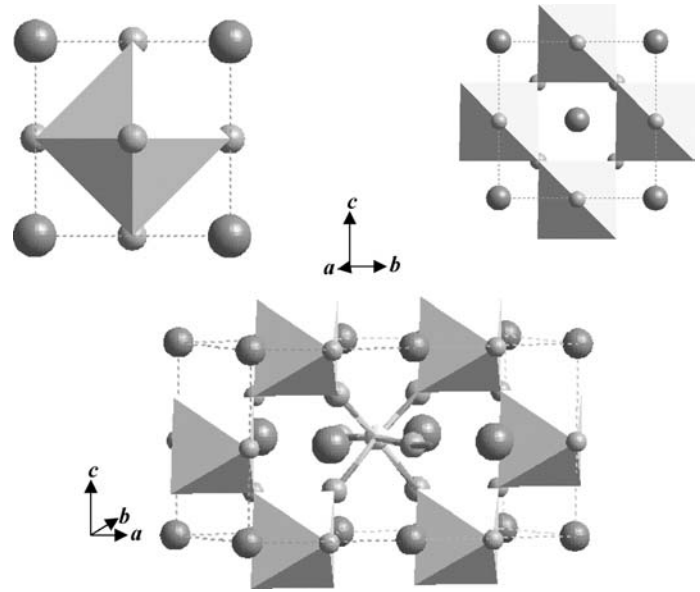


Table 1 Relationship between the surface structures investigated in this study (space group $Pbmm$) and the corresponding surfaces in the orthorhombic ($Amm2$) and cubic $Pm\bar{3}m$ perovskite structure of $BaTiO_3$

$Pbmm$	$Amm2$	$Pm\bar{3}m$
{001}	{100}	{100}
{101}	{102}	{111}
{111}	{101}	{201}
{011}	{111}	{112}
{110}	{011}	{001}

Plane wave methods

All plane wave calculations were undertaken with the CASTEP code (Payne et al. 1992; Lindan 1999),

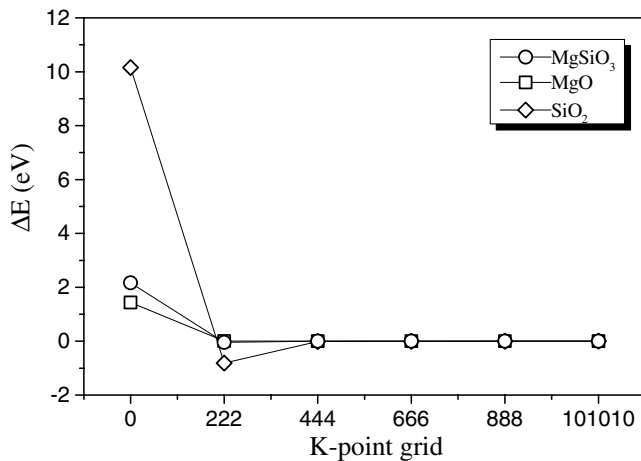


Fig. 3 Energy differences as a function of number of k-points for the different bulk structures investigated. We use an E_{cut} value of 380 eV. The total energies calculated for k-point grids of $10 \times 10 \times 10$ were used as reference values

employing the non-local ultrasoft pseudo-potentials available in the program (Payne et al. 1992; Vanderbilt 1990). The k-point grids employed are $6 \times 6 \times 6$ and $6 \times 6 \times 1$ for the bulk and surface calculations, respectively, and as demonstrated in Fig. 3 a k-point grid of $6 \times 6 \times 6$ is well converged for all the bulk structures investigated. The kinetic energy cut-off (E_{cut}) employed in all calculations was 380 eV. Lattice energies calculated with an E_{cut} of 380 eV resulted in an error of ~ 0.01 eV, compared to the higher E_{cut} value of 550 eV. In all calculations, we employed the Perdew-Wang91 (Perdew et al. 1992) functional described within the generalised-gradient approximation (GGA). In addition, the density-mixing method, as implemented in CASTEP, was applied.

Pair-potential methods

The atomistic calculations on the bulk structure were undertaken with the GULP program (Gale 1997; Gale 1996), while for the surface calculations we employed MARVIN'S program (Gay et al. 1999; Gay and Rohl 1995). In both GULP and MARVIN'S program the effective potentials describing the inter-atomic forces are represented by ionic, pair-wise potentials of the form:

$$U_{ij}(r_{ij}) = \frac{Z_i Z_j}{r_{ij}} + \sum_{ij} \varphi_{ij}$$

where the first term represents the Coulombic (long-range) interactions between each pair of ions in the crystal, and the second term describes the short-range interactions in the Buckingham potential:

$$\varphi_{ij}(r_{ij}) = b_{ij} \exp\left(-\frac{r_{ij}}{\rho_{ij}}\right) - \frac{c_{ij}}{r_{ij}^6}$$

For $MgSiO_3$, we employed two sets of inter-atomic potentials: the first potential (denoted P1; see Table 2)

Table 2 Inter-atomic potentials employed in the current work

Species	Charge	ij	A_{ij} (eV)	r_{ij} (Å)	C_{ij} (eV Å ⁶)
Shell-Potentials; P1					
Mg ^{ref}	+2	Mg-O _{shell}	1233.8032	0.29453	0.0
Si ^{ref}	+4	Si-O _{shell}	1383.735	0.32052	10.66158
O _{shell} ^{ref}	-2.848	O _{shell} -O _{shell}	22764.0	0.1490	27.88
O _{core} ^{ref}	+0.848				
Core-shell spring constants $k = 74.92$ eV Å ² in MgSiO ₃ O _{shell} -Si-O _{shell} three body spring constant $k = 2.09724$ eV rad ⁻¹ , short range cut off 12 Å					
Fixed Charge Ratio; P2					
Mg	+1.672	Mg-O	865.820	0.2866	0.0
Si	+3.344	Si-O	1422.019	0.2827	0.0
O	-1.672	O-O	2023.8	0.2674	13.83

was originally employed by Wall et al. and Wright et al. (Wright and Price 1993; Wright and Price 1989; Wall and Price 1989; Price et al. 1989; Wall et al. 1986; Watson et al. 2000) to model the bulk structure of MgSiO₃. In P1 formal charges (i.e. Si = +4, Mg = +2 and O = -2) are used in combination with a shell model on oxygen to simulate the polarisability of the oxygen ions. In addition, this model uses a three-body potential to induce directionality on the bonding around Si.

The second potential set (P2) used is a rigid ion one, with partial ionic charges (see Table 2). This potential was newly derived, and constrained the charge ratio between Mg and Si to be fixed to 1:2, so that this potential could be used to calculate neutral surfaces. The potential was derived employing the same technique as detailed by Oganov et al. (2000). The oxygen-oxygen potential was taken from Gavezzoti (1994), while the Z_{Si} , Z_{Mg} , b_{Si-O} and b_{Mg-O} were fitted to the experimental crystal structure at 1 atm and 300 K (Ross and Hazen 1989) and to the full elastic constant tensor (Yeganeh-Haeri 1994), using the GULP code (Z_O follows from $Z_O = -1/3(Z_{Mg} + Z_{Si})$). The ρ_{ij} values are fixed at the values calculated from the first ionisation potential (I_i) of atoms using the formula (Urusov 1975):

$$\rho_j = \frac{1.85}{\sqrt{I_i} + \sqrt{I_j}}$$

Table 3 Optimised structures and lattice energies of the GGA and inter-atomic potential calculations of MgSiO₃ perovskite, compared with experimental data and previous ab initio calculations.

Property	GGA*	P1*	P2*	LDA ^a	GGA ^a	Exp.
a (Å)	4.795	4.872	4.784	4.789	4.834 4.777	4.775 ^b
b (Å)	4.931	4.963	4.903	4.922	4.983 4.933	4.932 ^b
c (Å)	6.900	6.992	6.901	6.893	6.977 6.892	6.899 ^b
E_f (kJ/mol)	25.8	-45.7	-301.0	-	-	-
Bulk moduli (GPa)	-	322.88	281.97	257.8	231.3 266.7	264.0 ^c

^a Oganov et al. (2001)^b Ross and Hazen (1989)^c Yeganeh-Haeri et al. (1994)

The success that the P1 and P2 potentials have in reproducing the experimental and DFT data for the crystal structure of MgSiO₃ perovskite can be inferred from Table 3.

When simulating the MgSiO₃ structure, we need to reproduce the distortion and tilting of the SiO₆-octahedras as accurately as possible. In Table 4 the optimised Si-O distances are listed for the different theoretical models, and presented in comparison with the experimentally derived values. It is encouraging to see that the inter-atomic models employed for the MgSiO₃ structure reproduce the distortion of the SiO₆-octahedra satisfactorily. Likewise the DFT calculations also reproduce well the observed distortion of the SiO₆-octahedra.

Construction of surfaces

When creating the surfaces, we began from the geometry of the optimised bulk structures obtained from our inter-atomic potentials and DFT calculations. The surfaces were cut from the optimised bulk structure, and re-optimised, keeping the cell shapes and volumes fixed. In this way, a number of different low index surface structures were investigated, including the non-polar surfaces {001} and {110}, as well as the polar surfaces {111}, {101} and {011}. In addition, the perovskite

Values in *italics* denote temperature corrected lattice parameters and bulk moduli reported by Oganov et al. (2001), and star indicates current work

Table 4 Optimised tilting and distortion of SiO_6 -octahedra for MgSiO_3 perovskite employing the inter-atomic potentials described in the text in comparison to the experimental data and GGA calculations. Notations of the bond-distances (Si-O) and tilt angles ϕ are given in Fig. 1b

	P1	P2	GGA	Exp. ^a
Si-O _I	1.830	1.793	1.792	1.802
Si-O _{II}	1.818	1.778	1.791	1.791
Si-O _{III}	1.814	1.775	1.777	1.789
ϕ	145.5	148.5	148.6	146.2

^a Ross and Hazen (1989)

structure can be cleaved in several different planes, representing different MgO- and SiO_2 -terminations, e.g. for the $\{011\}$ surface we constructed one type of MgO- and two types of SiO_2 -terminated surfaces, and for the $\{111\}$ and $\{101\}$ surfaces we created two MgO- and SiO_2 -types of surfaces. Consequently, the surface terminations of the different surfaces have to be carefully investigated. In Table 4 we show examples of different surface terminations examined here.

A particular problem is caused by the polar $\{111\}$, $\{101\}$ and $\{011\}$ surfaces, which are usually less stable than the non-polar surfaces, and are known to undergo complicated surface reconstructions (Heinrich and Cox 1996). There are many possible surface structures of these polar surfaces, and because of their complexity, only the non-reconstructed surfaces were considered in the current study, i.e. those surfaces that can be cut out from the geometry optimised bulk structure.

Static lattice simulations

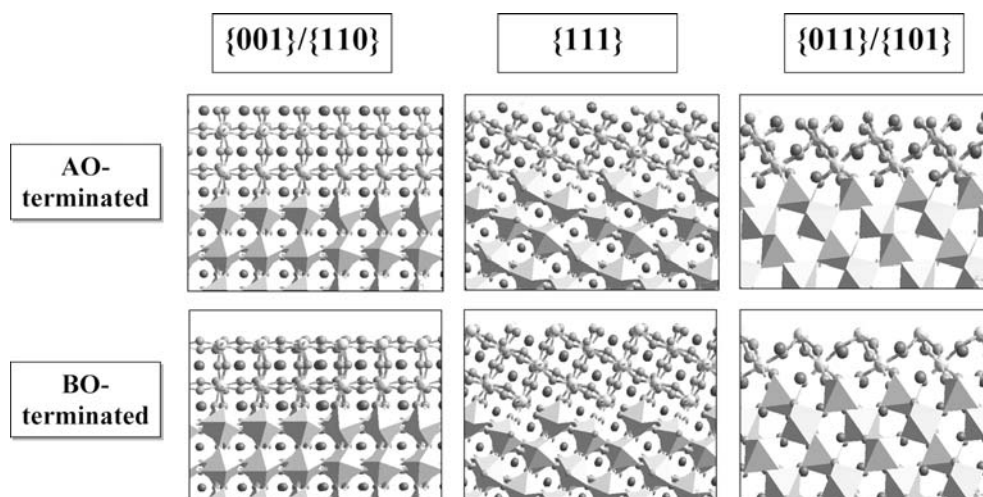
In MARVIN'S program, the simulated slabs are periodic in two dimensions (x and y) with a finite thickness in the third z-direction, corresponding to the direction perpendicular to the surface. Furthermore, the slab is divided into two regions, a region in which all the atomic

coordinates are fully relaxed, and a second region in which the atomic coordinates are kept fixed to the optimised bulk values. These are denoted as Region I and II, respectively. In all calculations, the size of Region I was carefully investigated to make sure that the atomic displacements are completely relaxed and that surface energies were converged with respect to regions of larger thickness. We found that for a slab thickness of 16 surface layers for the $\{001\}$ surfaces (see Figs. 4a and b), the surface energies and optimised distances are well converged. However, in all calculations we employed slab thicknesses of Regions I and II corresponding to 28 and 56 surface layers, respectively. For all calculations employing MARVIN'S program we used a 2×2 supercell, to allow for the possibility of commensurate surface reconstructions. We found, however, that surface energies only differ by ca. 0.002 J/m^2 between the 2×2 and 1×1 supercells of the $\{001\}$ surfaces, suggesting that no surface reconstructions are observed in the computational cell.

Plane wave methods

The periodic boundary conditions employed by CASTEP require the surfaces to be modelled as repeated slabs, separated by a 'pseudo-vacuum'. In the current study a pseudo-vacuum of 10 \AA was applied. The $\{001\}$ terminated slabs are Type 1 surfaces (Tasker 1979), but due to the low symmetry, a dipole moment exists perpendicular to the surfaces (see Fig. 5). This makes the SCF cycles very difficult to converge, and to avoid this problem the slabs were constructed to have a central plane of symmetry, that therefore gave two equivalent surfaces (Fig. 5c). As for the atomistic simulations, we optimised the thickness of the slab to make sure that surface energies and atomic displacements were fully converged. We found that surface energies are well converged for the $\{001\}$ surface (see Fig. 6), employing a slab thickness of 17 surface layers.

Fig. 4a–c Representative surface structures before geometry optimisation of the **a** $\{001\}$ and $\{110\}$, **b** $\{111\}$ and **c** $\{011\}$ and $\{101\}$ surfaces of MgSiO_3 perovskite. For each MgO- and SiO-terminated surface one example is presented. Dark grey, light grey and white balls indicate Mg, O and Si, respectively. SiO_6 -octahedra marked in light grey. A and B in the text boxes represent Mg and Si, respectively



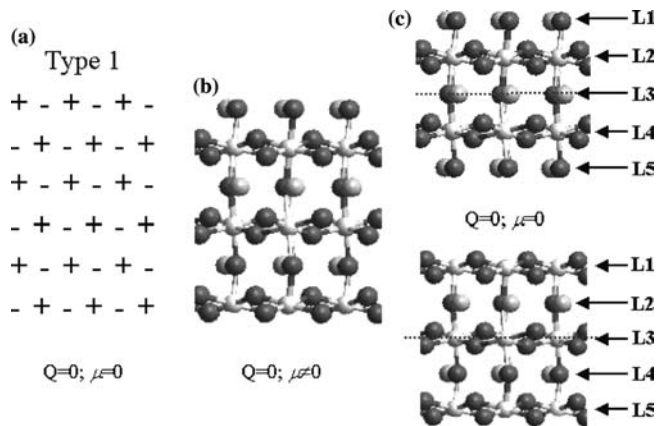


Fig. 5 a Schematic picture of a Type 1 surface according to Tasker (1979). Q denotes total charge of surface layer, and μ the dipole moment. b $\{001\}$ slab containing both an MgO and SiO₂-terminated surface. c The upper figure shows a slab containing two MgO-terminated surfaces, and the lower figure a slab with two SiO₂-terminated surfaces. Both slabs contain a mirror plane, indicated as dashed lines. Numbering of surface layers is given

Surface energies

The fact that we are required to use slabs with two equivalent surfaces in our plane wave calculations results in having surfaces that have different numbers of MgO and SiO₂ formula units in the surface slabs and in the bulk unit cell. One must therefore be careful when calculating the energies of such MgO- and SiO₂-terminated surfaces. In this paper, we quote surface energies obtained from the average energy for the two types of termination, thus:

$$E_{surf} = \frac{\frac{1}{4} (E_{slab}^{MgO} + E_{slab}^{SiO_2} - nE_{bulk})}{\text{Surface Area}} \quad (1)$$

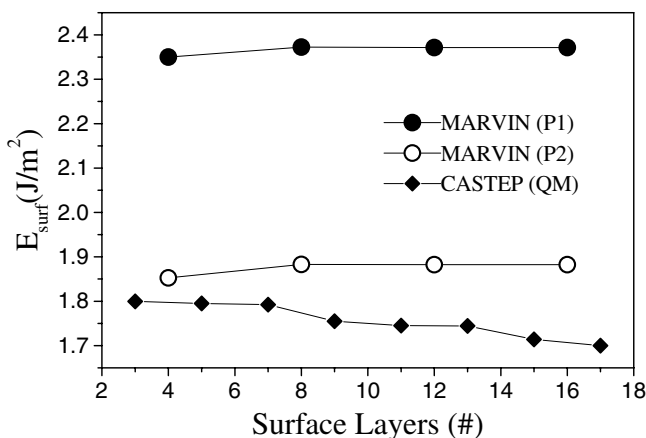


Fig. 6 Surface energies for the P1, P2 and GGA models of MgSiO₃. Surface energies reported are the average surface energy of the MgO- and SiO₂-terminated surfaces, calculated according to equation 1 and 2 for the CASTEP and MARVIN'S calculations, respectively. Energies given in J/m²

where the factor of 1/4 comes from the fact that we create four surfaces in the cleavage procedure (see Fig. 5c), and the factor n corresponds to the number of formula units of MgSiO₃ in the bulk. E_{bulk} is the total energy of the primitive unit cell of the perovskite structure calculated under the same conditions as the slabs.

Obtaining surface energies as a function of surface termination in MARVIN'S program is more straightforward, as they are obtained from:

$$E_{surf} = \frac{E_{slab} - nE_{bulk}}{\text{Surface Area}} \quad (2)$$

where E_{slab} is the total energy of the slab with various surface terminations.

Comparison between lattice static and plane wave surface calculations

To investigate the transferability of the pair-potentials from bulk to surface calculations we started by comparing the average surface energies of the MgO and SiO₂-terminated $\{001\}$ surfaces (employing equation 2) calculated using the inter-atomic potential models (P1 and P2) with the value obtained using our high level ab initio calculations (employing equation 1). In Fig. 6 we present average surface energies for the MgO and SiO₂-terminated $\{001\}$ surfaces obtained within the GGA Hamiltonian as well as the inter-atomic potential based P1 and P2 models. It can be seen that the P1 model overestimates the surface energies compared with the DFT calculations by about 30% (0.5 eV). In contrast surface energies calculated with our P2 model are only overestimated by ca. 10% (0.2 eV) relative to the surface energies obtained from our GGA calculations.

In general, surface energies increase with decreasing ion size and increasing ionic charge. An example of this behaviour is demonstrated by Kotomin et al. (2001). In their study (on SrTiO₃ thin films) it is reported that the different DFT Hamiltonians all result in effective charges and surface energies in good agreement to each other. In contrast HF calculated charges are (as expected) higher than those reported for the DFT methods, and the reported surface energies are correspondingly overestimated compared with those obtained with the DFT methods. The higher surface energies calculated with the P1 inter-atomic potential set are therefore probably related to the use of formal charges in this model.

Another important contribution to the surface energy is made by the geometric relaxations of the surfaces when they are created. Here we calculate the relaxation energies of the $\{001\}$ surfaces for the P1, P2 and GGA simulations to be 0.723, 0.776 and 2.186 J/m² for the SiO₂-terminated, and 1.185, 0.630 and 0.771 J/m² for the MgO-terminated surfaces, respectively. The sizes of these energetic contributions are less systematic, and so

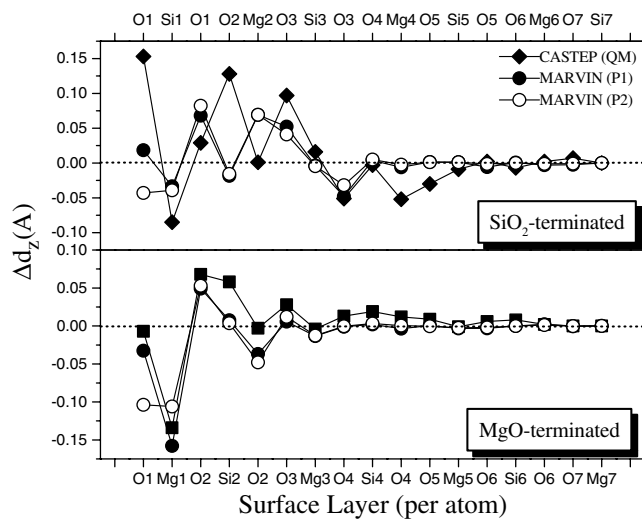
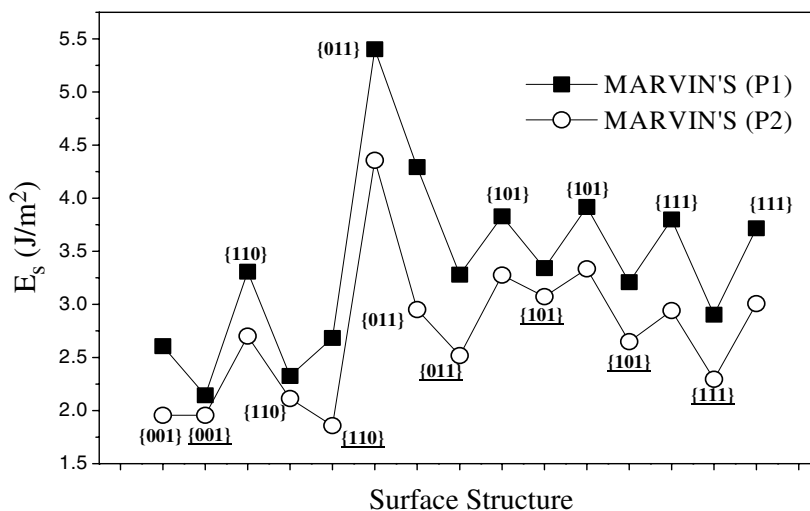


Fig. 7 Surface displacements in the z -direction for the $\{001\}$ surfaces of MgSiO_3 perovskite compared to the non-optimised surface structures, employing different computational models. The upper figure represents the SiO_2 -terminated surfaces and the lower part the MgO -terminated surfaces. Negative displacements indicate inward translations

affect the total calculated surface energies in a less predictable way.

To establish the complete behaviour of the inter-atomic potential models we also report surface displacements perpendicular to the surface plane for the $\{001\}$ surfaces (see Fig. 7). Analysing the displacements of the geometry optimised surfaces relative to the non-geometry optimised structures, we find that the P1 model reproduces the same behaviour as the GGA calculations, while the P2-calculations fail to reproduce the rumpling of both the MgO - and SiO_2 -terminated surfaces. Potential set P2 predicts an outward relaxation for only one type of the O-ions, while both the GGA and P1 calculations show that the two types of O-ions are outwardly relaxed, while the Si-ions are inward relaxed on the SiO_2 -terminated surface

Fig. 8 Surface energies calculated with the P1 and P2 models for the MgSiO_3 structure. Underlined surface structures denote MgO -terminated surfaces



(see Fig. 4b). For the MgO -terminated surface (see Fig. 4a) both the O and Mg ions are inwardly relaxed with similar displacements. Although the surface displacements observed for the P1 potential are smaller than the surface relaxations predicted with our GGA calculations, the P1 potential gives the same relative directions for both the MgO - and SiO_2 -terminated surfaces as the DFT calculations, and the rumpling of the surfaces is, therefore, similar. The source of the failure of the surface displacements with the P2 model is likely to originate from the rigid ion oxygen potential used in this model, which fails to reproduce the polarisability of the surface oxygens.

To conclude, we find that it is clearly important to use a shell-model to correctly reproduce the polarisation of the oxygen ions at the surface structure, and all atomistic simulations in the results section are undertaken with the P1 potential except in Section 4.1 where we make further comparisons between the P1 and P2 potentials.

Results

Surface stabilities

We commenced our investigation by performing a number of inter-atomic potential calculations on low index non-polar surfaces (see Fig. 4), including various surface terminations, denoted MgO - or SiO_2 -terminated depending on the ionic species dominating the surface layer. As can be seen from Fig. 8 the most stable surface, employing the P1 model, is the MgO -terminated $\{001\}$ surface. The next most stable surface is the MgO -terminated $\{110\}$ surface, which has a surface energy that is only 0.3 J/m^2 higher than that of the $\{001\}$ surface—a result that follows from the similarity in the structures of the two surfaces.

The polar $\{111\}$, $\{101\}$ and $\{011\}$ surfaces of perovskites are known to reconstruct to sustain charge

neutrality. These reconstructions are often complicated and depend on the environment, such as oxidising or reducing nature of the atmosphere. However, here we present a number of different unreconstructed surface structures, and we find that these polar surfaces also favour an MgO-termination, with surface structures similar to those shown in the upper part of Fig. 4. Indeed for the P1 potential, all the surfaces we investigated showed that the MgO-termination is more favourable than the SiO₂-terminated surfaces. We also find that the surface energies (see Fig. 8) for the different SiO₂-terminated {101} and {111} surfaces are similar, which is related to the similar surface structures after relaxation. We have no experimental data with which to compare our optimised polar surfaces of MgSiO₃, and it is, therefore, difficult to resolve the true structures of these surfaces: i.e. to establish whether they undergo large surface reconstructions or remain essentially unreconstructed.

For comparison we also show the results obtained for model P2 in Fig. 8, and it can be seen that in fact that both potentials P1 and P2 predict the same relative order of the surface energies. We are, therefore, confident that surface structures and predicted morphologies (discussed in Section 5 below) show the correct general behaviour, even though the absolute surface energies are overestimated with the P1 model compared with those obtained with the GGA and P2 simulations (*see* Fig. 6). The largest discrepancy between the P1 and P2 potential is demonstrated for the {001} and {110} surfaces, which can be associated with the different surface relaxations of the P2 model compared to the P1 and GGA calculations discussed above.

Surface geometries

In the current section we analyse the surface relaxations listed in Table 5. In this table, we report the surface displacements both within the plane of the surface (i.e. in the x- and y-directions) as well as perpendicular to the surfaces (z-direction). In summary, we find that for both the MgO- and SiO₂-terminated {001} surfaces the cations (Mg²⁺ and Si⁴⁺) are inwardly relaxed perpendicular to the surface plane, while the O²⁻ ions show smaller displacements often within the surface plane. Consequently, both the SiO₂- and the MgO-terminated structures are oxygen terminated. Additionally, it can be seen that the SiO₂-terminated surface shows larger relaxations than the MgO-terminated surface. Hence, the latter surface termination causes a smaller overall structural perturbation.

Owing to the similarity of the structures of the {001} and {110} surfaces we expect these surfaces to behave in a comparable way, but as consequence of symmetry the outermost Mg²⁺ ions on the {110} surface only displace within the x- and z-directions, while on the {001} surface the translation of the Mg²⁺ ions occur also in the y-direction.

Table 5 Surface displacements for the outermost layers within the x-, y- and z-directions for the energetically most stable surface structures. For the {001} surface both the MgO- and SiO₂-terminated surfaces are included. Positive and negative values indicate outward and inward translations, respectively compared to the non-optimised surfaces

Surface ion	x	y	z
{001} / MgO-terminated			
Mg	(±)0.193	-0.112	-0.158
O _I	(±)0.034	0.099	-0.033
{001} / SiO ₂ -terminated			
O _{II}	(±)0.176	0.146	0.019
Si	(±)0.087	-0.027	-0.034
O _{III}	(±)0.206	-0.238	0.068
{110} / MgO-terminated			
O _I	-0.133	(±)0.038	-0.023
Mg _I	0.167	0.	-0.162
O _{II}	0.071	(±)0.050	0.005
Mg _{II}	-0.426	0.	-0.167
{111} / MgO-terminated			
Mg	0.204	0.099	-0.261
O _I	0.069	0.011	-0.086
O _{II}	0.672	-0.103	0.031
{011} / MgO-terminated			
Mg	-0.054	0.177	-0.067
O _I	0.196	0.322	0.013
O _{II}	-0.107	0.009	-0.005
{101} / MgO-terminated			
O _I	(±)0.127	0.148	-0.293
Mg	(±)0.035	0.311	-0.161
O _{II}	(±)0.233	0.431	0.221

In Table 5 we also report surface displacements of the energetically most stable unreconstructed polar surfaces. Our inter-atomic potential calculations on these surfaces again show important displacements perpendicular to the surface, but also important relaxations within the surface plane, resulting in surface structures with higher density than in the non-relaxed surfaces. As on the {001} and {110} surfaces we find the {101}, {011} and {111} surfaces are oxygen terminated.

Comparison with other perovskite systems

Surface energies for different surface terminations of the cubic and tetragonal structures of SrTiO₃, BaTiO₃ and PbTiO₃ are reported in Padilla and Vanderbilt (1998), Padilla and Vanderbilt (1997), Kotomin et al. (2001), Heifets et al. (2001), Heifets et al. (2000) and Meyer et al. (1999). Heifets et al. (2000) report inter-atomic potential calculations on the {100} surfaces of the cubic perovskite SrTiO₃, employing MARVIN'S program. In this latter investigation the SrO-terminated {001} surface is reported to be the energetically most stable surface ($E_s = 1.32 \text{ J/m}^2$), in agreement with our calculations on MgSiO₃ for which the MgO-terminated {001} surface is the energetically most stable surface ($E_s = 2.2 \text{ J/m}^2$). However, plane wave calculations by Vanderbilt's group (Meyer et al. 1999; Padilla and Vanderbilt 1998), formulating the surface energy as a function of the chemical potential of TiO₂, predict that when the TiO₂-terminated

{001} surfaces of SrTiO₃ are in direct contact with the binary oxide of TiO₂, they are energetically favoured over the SrO-termination. Similar behaviour is reported for BaTiO₃, while for PbTiO₃ the PbO-termination is the only favourable surface termination (Meyer et al. 1999).

Polar surfaces of the cubic structures of SrTiO₃ (Pojani et al. 1999a; Heifets et al. 2001; Heifets and Kotomin 2000) and BaTiO₃ (Heifets et al. 2000) have also been investigated computationally. In a detailed study by Pojani et al. (1999a) on the unreconstructed and reconstructed polar surfaces of SrTiO₃, the {111} surfaces are reported to be energetically less sensitive to the different types of surface terminations than the {110} surfaces, i.e. for the {111} surfaces the calculated surface energies are all close to ~ 2.5 J/m² independent of the surface composition, while for the {110} surface energies vary between 1.1 and 3.1 J/m² dependent on surface geometry and stoichiometry. For the polar surfaces of MgSiO₃ we find a similar behaviour: the {111} surface (structural equivalent to the {111} surface of SrTiO₃) is less structure-sensitive than the {011} surface (comparable with the {110} surface of SrTiO₃) as shown in Fig. 8. One of the {011} surfaces is Si-terminated, and as such it contains unsaturated bonds. Consequently, it has a higher surface energy ($E_s \sim 5.5$ J/m²) than the other surface terminations. We know from silica (Koudriachova et al. 2001; Bart and Gautier 1994; Legrand 1999) and silicon (Nörenberg and Briggs 1999; Çakmak and Srivastava 2003) that these surfaces readily reconstruct or form different types of hydroxylated surfaces (de Leeuw et al. 1999; Litton and Garofalina 2001; Mazzara et al. 1999; Legrand 1999). With the exception of the Si-terminated surfaces, the energies of all the other polar surfaces studied are not unreasonably large, only being about 1.5 J/m² higher than the non-polar surfaces, an observation that agrees with the surface energies calculated for SrTiO₃ and BaTiO₃.

Experimental studies on BaTiO₃ (Lo and Samorjai 1977; Ferrer and Samorjai 1980; Tanaka and Kawai 1996; Sigmund et al. 1997; Sekiguchi et al. 1998; Hagedorf et al. 1998) and SrTiO₃ (Bando et al. 1995; Brunen and Zegenhagen 1997; Erdman et al. 2002) show that under oxidising and reducing conditions complicated surface reconstructions may occur, resulting in both AO_{3-x}- and TiO_x-terminated surfaces. However, in a number of the latter investigations unreconstructed polar surfaces are also reported, while other oxides such as MgO only show reconstructed polar {111} surfaces (Heinrich 1976). The reason for this is believed to be that the ATiO₃ perovskites form insulating polar surfaces, while the polar {111} surface of MgO is found to be metallic and as such less stable than the insulated surfaces of ATiO₃ (Pojani et al. 1999b).

Morphology

It has been suggested (e.g. Karato et al. 1992, 1995) that the dominant mechanism for the deformation of

MgSiO₃-perovskite in the lower mantle will depend on its grain size; i.e. deformation of small grain size aggregates occurs by diffusion or superplastic creep, whereas dislocation creep or twinning will be favoured in larger grain size assemblages. Hence, the rheological properties of the lower mantle are likely to be affected by the grain size and shape of MgSiO₃-perovskite. Although the grain shape in a dynamically deforming system will be different from that of its equilibrium morphology, it is generally true that at moderate strain rates minerals that develop equant equilibrium morphologies do not develop large shear induced morphological anisotropy. Although the shape of MgSiO₃-perovskite crystals developed in a convecting mantle cannot yet be established, it is possible to calculate its equilibrium crystal morphology. This crystal morphology is also important for understanding the reactivity of MgSiO₃-perovskite, i.e. if the exposed crystal habits are polar (reactive) or non-polar (less reactive) surface structures.

In the current investigation we employ three different models to predict the morphology, i.e. the Bravais-Friedel-Donnay-Harker (BFDH) model, the Equilibrium model and the Growth model (Gay and Rohl 1995). In the BFDH model, the morphology is obtained by analysing the crystal structure (cell parameters and space group), assuming that surfaces with large inter-planar distances (d_{hkl} -values) control the crystal morphology, because the growth rates of these faces are the rate determining growth steps. In the Equilibrium model the morphology is derived from calculated surface energies and their orientation dependence to the crystallographic axes. Making the assumption that faces with the lowest surface energies and largest inter-planar distances control the growth rate and that these surfaces determine the crystal morphology. In the Growth model the growth rates of the surface planes are predicted from the attachment energies, defined as the energy gained when a 'growth slice' is attached to a face of the growing crystal. The growth rate of a given crystal face is taken to be proportional to the absolute value of the attachment energy, and so faces with the lowest attachment energies will be the slowest growing and have the most morphological importance.

The predicted morphologies obtained by employing these three models are shown in Fig. 9. It can be seen that both the BFDH and Equilibrium models (Figs. 9a and b) predict a faceted morphology, while the Growth model predicts a rectangular prismatic morphology (Fig. 9c). However, analysing the surface areas it is found that for all three models the dominating faces are the {001} and {110} surfaces, which we have shown above have equivalent surface energies owing to the similarity of their surface structures (see Fig. 4). Because the dominating surface structures are the energetically most stable non-polar surfaces (see Fig. 8) MgSiO₃-perovskite crystals are expected to be less reactive than if the polar surfaces were the dominating surfaces.

Fig. 9a–c Predicted morphology of the perovskite structure of MgSiO_3 , employing **a** the BFDH, **b** the Equilibrium, and **c** the Growth models. All calculations are undertaken with the P1 model. The different surface structures are denoted in the figures

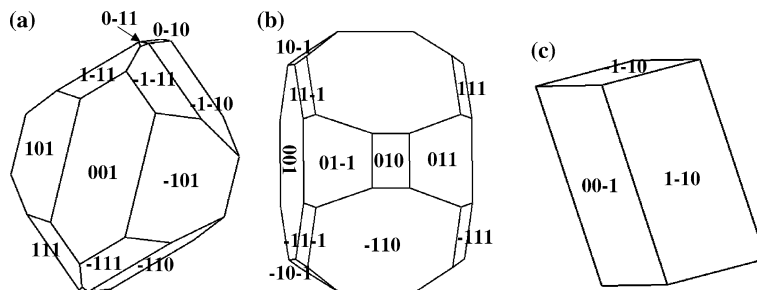


Fig. 10 shows a scanning electron microscopy (SEM) image of flux-grown MgSiO_3 perovskite crystals. These crystals were grown from a starting synthetic perovskite of composition $0.997(\text{MgSiO}_3)0.003(\text{NaSiO}_{2.5})$, which was loaded in a NaCl pressure medium and recrystallised at 24 GPa and 1950°C for 30 min. NaCl is a liquid under these experimental conditions and idiomorphic perovskite crystals grew by a solution-precipitation process. The resultant MgSiO_3 perovskite shows a dominant prismatic to cubic habit with minor octahedral facet development. This can be produced by development of $\{001\}$, $\{010\}$ and $\{100\}$ pinacoids with $\{111\}$ form, or $\{001\}$ pinacoid with $\{110\}$, $\{101\}$ and $\{011\}$ forms of the pseudocubic setting in orthorhombic ($Pbmm$) symmetry, the latter being consistent with Fig. 9e. The flux-grown MgSiO_3 crystals in general exhibit a particle size of ca. 200 μm . Previous observations suggest that the morphologies predicted from the Growth model are often found to reproduce best the experimental observations considering larger crystal and geological species, while the Equilibrium model morphology often agrees better with experimentally grown crystals that are less than a micron in diameter (Gay and Rohl 1995). Hence, crystal particles, exhibiting particle sizes of less than 1 μm , grown by mechanically pressing powders of the analogue CaTiO_3 perovskite structure at different temperatures, exhibit faceted structures

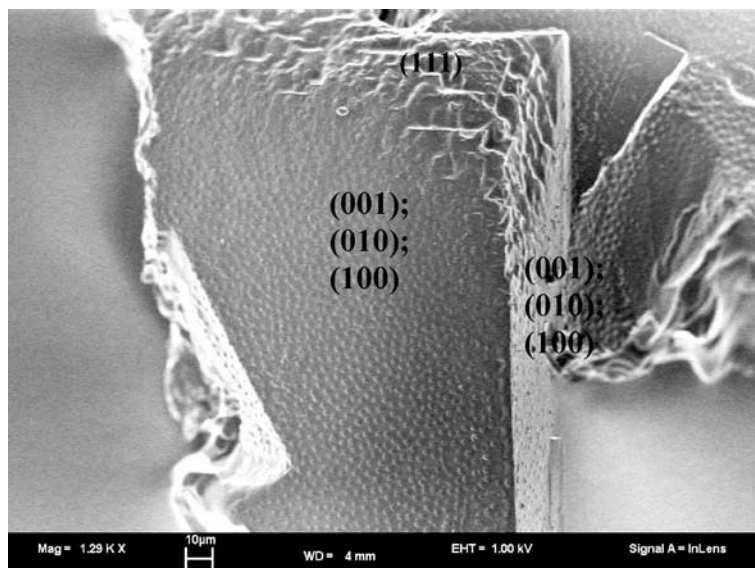
comparable with the morphologies predicted with the BFDH and Equilibrium models (Wang et al. 1999).

Because the crystal morphology is environmentally dependant, the different models we have used to predict crystal habits all seem in general agreement with experimentally observed perovskite morphologies. More work is needed on the theory of crystal growth before the appropriateness of the competing models can be effectively established.

Summary

This paper is the first in a series in which we aim to investigate the surface structures and grain boundaries of MgSiO_3 perovskite. Surface simulations are computationally demanding, and so one would wish to do them with computationally efficient simulations, but one needs also to establish the accuracy of the simulation. In this study we have confirmed that simulations of perovskite surfaces can be done using effective interatomic potential calculations, and that these simulations predict the same behaviour as more computationally intensive high level ab initio methods. Our calculations show that it is important to employ a shell-model potential to correctly reproduce the surface structures. However, to reproduce surface energies, in agreement

Fig. 10 Scanning electron microscopy (SEM) picture of one MgSiO_3 perovskite crystal (for experimental details see the text). A few of the possible surface indices are included in the picture, but no surface determination has yet been undertaken, and all the different combinations of the surface indices should, therefore, be considered



with GGA calculations, the potential should be derived with partial charges on the ionic species.

Our atomistic simulations predict the MgO-terminated {001} surface to be the energetically most stable surface for MgSiO₃ perovskite. As expected, the SiO₂-terminated surfaces are less stable than the MgO-terminated surfaces, because the SiO₂-terminated surfaces contain unsaturated Si-bonds. As a result of surface relaxations, all the surfaces we investigated are oxygen terminated. For the polar {111}, {101} and {110} surfaces we also find that the ionic displacements result in more dense surface structures than observed for the unrelaxed surfaces.

In the future we intend to investigate the grain boundary structures of MgSiO₃ perovskite. For this we need to know the most probable surfaces exhibited by MgSiO₃ perovskite, and so we employed three different models to predict its most likely morphology. All three models showed that the largest proportion of the perovskite surface is likely to be dominated by {001} and {110} faces. However, dependent on the model we use, we predict a faceted or prismatic morphology for this mineral. SEM pictures of the analogue structure CaTiO₃ show faceted crystal particles in good agreement with our BFDH and equilibrium models, while the Growth model shows better agreement with flux grown crystals of MgSiO₃ perovskite. Because the crystal morphology is environmentally dependent, we conclude that our predicted crystal morphologies are plausible, and we await more experimental studies on perovskite morphology before we can differentiate between the varieties of competing morphology models currently available.

Acknowledgements We wish to thank S. Jacobsen and F. Heidebach for assistance in collecting the SEM image of the flux-grown MgSiO₃ crystal, and D. S. Coombes, F. Corà and K.W. Wright for valuable discussions. Financial support from NERC is gratefully acknowledged (grant No(s): NER/T/S/2001/00855; NER/O/S/2001/01227 and GR9/02072). We are also thankful to EPSRC and NERC for the computer facilities provided at the Royal Institution of Great Britain, University College London, Bath University and the High Performance Computing facilities of the University of Manchester. DPD is grateful for fellowships from the Alexander von Humboldt Stiftung and the Royal Society.

References

- Andraut D, Bolfan-Casanova N, Guignot N (2001) Equation of state of lower mantle (Al,Fe)-MgSiO₃ perovskite. *Earth Planet Sc. Lett.* 193:501–508
- Bando H, Aiura Y, Haruyama Y, Shimizu T, Nishihara Y, (1995) Structure and electronic states on reduced SrTiO₃(110) surface observed by scanning tunneling microscopy and spectroscopy. *J. Vac. Technol. B* 13:1150–1154
- Bart F and Gautier M (1994) A LEED study of the (0001) a-quartz surface reconstruction, *Surf. Sci.* 311: L671-L676
- Bolfan-Casanova N, Keppler H, Rubie DC, (2002) Hydroxyl in MgSiO₃ akimotoite: A polarized and high-pressure IR study. *Am. Mineral* 87(5–6): 603–608
- Brunen J and Zegenhagen J (1997) Investigation of the SrTiO₃ (110) surface by means of LEED, scanning tunneling microscopy and Auger spectroscopy. *Surf. Sci.*, 389:349–365
- Çakmak M and Srivastava GP (2003) Theoretical study of dangling-bond wires on the H-terminated Si surface, *Surf. Sci.* 532–535:556–559
- Chen JH, Weidner DJ and Vaughan MT (2002) The strength of Mg_{0.9}Fe_{0.1}SiO₃ perovskite at high pressure and temperature. *Nature* 419 (6909): 824–826
- de Leeuw NH, Higgins FM and Parker SC (1999) Modelling the surface structures and stability of α -quartz, *J. Phys. Chem. B* 103:1270–1277
- Erdman N, Poppelmeier KR, Asta M, Warschkow O, Ellis DE and Marks LD (2002) The structure of the TiO₂-rich surface of SrTiO₃(001). *Nature* 419:55–58
- Fei YW and Wang YB (2000) High-pressure and high-temperature powder diffraction. *Rev. Mineral. Geochem.* 41:521–557
- Ferrer S and Samorjai GA (1980) Isotope exchange studies of the oxidation and reduction of SrTiO₃ single crystal surfaces by water and hydrogen. *Surf. Sci.*, 97: L304-L308
- Fiquet G, Andraut D, Dewaele A, Charpin T, Kunz M and Hausermann D (1998) P-V-T equation of state of MgSiO₃ perovskite *Phys. Earth Planet. Int.* 105:21–31
- Fiquet G, Dewaele A, Andraut D, Kunz M and Le Bihan T (2000) Thermoelastic properties and crystal structure of MgSiO₃ perovskite at lower mantle pressure and temperature conditions. *Geophys Res. Lett.* 27:21–24
- Gale JD (1996) Empirical potential derivation for ionic materials. *Phil. Mag. B*, 73:3-19
- Gale JD (1997) GULP—a computer program for the symmetry adapted simulation of solids. *JCS Faraday Trans.* 93:629–637
- Gavezotti A (1994) Are crystal structures predictable? *Acc. Chem. Res.* 27:309–314
- Gay DH, Rohl AL, Nygren MA, Slater B and Whitmore L (1999) MARVIN'S Program. The Royal Institution of Great Britain, London, UK: www.ri.ac.uk/DFRL/MARVIN
- Gay DH and Rohl AL (1995) MARVIN: A new computer code for studying surfaces and interfaces and its application to calculating the crystal morphologies of corundum and zircon. *J. Chem. Soc. Farad. Trans.* 91:925–936
- Hagendorf C, Schindler KM, Doege T and Neddermeyer H (1998) An STM, XPS and LEED investigation of the BaTiO₃(111) surface. *Surf. Sci.*, 402–404:581–585
- Heifets E, Eglitis RI, Kotomin EA, Maier J and Bortsel G. (2001) Ab initio modelling of surface structure for SrTiO₃ perovskite crystals. *Phys. Rev. B* 64:235417(1–5)
- Heifets E and Kotomin EA (2000) Atomistic simulations of SrTiO₃ and BaTiO₃ (110) surface relaxations. *Thin Solid Films* 358:1-5
- Heifets E, Kotomin EA and Maier J (2000) Semi-empirical simulations of surface relaxation for perovskite titanates, *Surf. Sci.*, 462: 19–35
- Heinrich VE (1976) Thermal faceting of (110) and (111) surfaces of MgO. *Surf. Sci.* 57:385–392
- Heinrich VE and Cox PA (1996) *The Surface Science of Metal Oxides*. Cambridge University Press, Cambridge, UK
- Karato SI, Zhang S and Wenk HR (1995) Superplasticity in Earth's Lower Mantle: Evidence from Seismic Anisotropy and Rock physics. *Science* 270:458–461
- Karato SI and Li P (1992) Diffusion creep in Perovskite: Implications for the rheology of the lower mantle. *Science* 255:1238–1240
- Karki BB, Stixrude L, Wentzcovitch RM (2001) High-pressure elastic properties of major materials of Earth's mantle from first principles. *Rev. Geophys.* 39:507–534
- Karki BB, Wentzcovitch RM, de Gironcoli S and Baroni S (2000) Ab initio lattice dynamics of MgSiO₃ perovskite at high pressure. *Phys. Rev. B* 62:14750–14756
- Kotomin EA, Eglitis RI, Maier J and Heifets E (2001) Calculations of the atomic and electronic structure for SrTiO₃ perovskite thin films. *Thin Solid Films* 400:76–80
- Koudriachova MV, Beckers JVL, de Leeuw SW (2001) Computer simulation of the quartz surface: a combined ab initio and empirical potential approach, *Comp. Mat. Sci.* 20:381–386

- Legrand AP ed. (1998) The surface properties of silicas, John Wiley & Sons, Chichester, UK
- Lindan P (1999) The Guide 1.1 to CASTEP 3.9. Daresbury Laboratory, Warrington, UK
- Litton DA and Garofalini SH (2001) modeling of hydrophilic wafer bonding by molecular dynamics simulations, *J. Appl. Phys.* 89:6013–6023
- Lo WJ and Samorjai GA (1977) Temperature-dependent surface structure, composition, and electronic properties of the clean SrTiO₃(111) crystal face: Low-energy-electron diffraction, Auger-electron spectroscopy, electron energy loss, and ultraviolet-photoelectron spectroscopy studies. *Phys. Rev. B* 17:4942–4950
- Marton FC and Cohen RE (2002) Constraints on lower mantle composition from molecular dynamics simulations of MgSiO₃ perovskite. *Phys. Earth Planet. In.* 134:239–252
- Matsui M (2000) Molecular dynamics simulation of MgSiO₃ perovskite and the 660-km seismic discontinuity. *Phys Earth Planet In.* 121:77–84
- Mazzara C, Jupille J, Zheng WQ, Tanguy M, Tadjeddine A and Dumas P (1999) Hydrogen-terminated Si(111) and Si(100) by wet chemical treatment: linear and non-linear infrared spectroscopy, *Surf. Sci.* 427–428:208–213
- Meyer B, Padilla J and Vanderbilt D (1999) Theory of PbTiO₃, BaTiO₃, and SrTiO₃ surfaces. *Faraday Disc. No.* 114:395–405
- Nörenberg H and Briggs GAD (1999) The Si(001) c(4×4) surface reconstruction: a comprehensive experimental study, *Surf. Sci.* 430:154–164
- Oganov AR, Brodholt JP and Price GD (2000) Comparative study of quasiharmonic lattice dynamics, molecular dynamics and Debye model applied to MgSiO₃ perovskite. *Phys. Earth and Plan. Inter.* 122:277–288
- Oganov AR, Brodholt JP and Price GD (2001) The elastic constants of MgSiO₃ perovskite at pressures and temperatures of the Earth's mantle. *Nature* 41:934–937
- Padilla J and Vanderbilt D (1998) Ab initio study of SrTiO₃ surfaces. *Surf. Sci.* 418:64–70
- Padilla J and Vanderbilt D (1997) Ab initio study of BaTiO₃ surfaces. *Phys. Rev. B* 56:1625–1631
- Parlinski K and Kawazoe Y (2000) Ab initio study of phonons and structural stabilities of the perovskite-type MgSiO₃. *Eur. Phys. J. B* 16:49–58
- Payne MC, Teter MP, Allan DC, Arias TA and Joannopoulos JD (1992) Iterative minimization techniques for ab initio total-energy calculations: molecular dynamics and conjugate gradients. *Rev. Mod. Phys.* 64:1045–1097
- Perdew JP, Chevary JA, Vosko SH, Jackson KA, Pederson MR, Singh DJ and Fiolhais V (1992) Atoms, molecules, solids, and surfaces: Applications of the generalized gradient approximation for exchange and correlation. *Phys. Rev. B* 46:6671–6687
- Pojani A, Finocchi F and Noguera C (1999a) Polarity on the SrTiO₃ (111) and (110) surfaces. *Surf. Sci.* 442:179–198
- Pojani A, Finocchi F and Noguera C (1999b) A theoretical study of the unreconstructed polar (111) face of SrTiO₃. *Appl. Surf. Sci.* 142:177–181
- Price GD, Wall A and Parker SC (1989) The properties and behaviour of mantle minerals – a computer-simulation approach. *Phil. Trans. of the Royal Society of London series A-Mathematical physical and engineering sciences* 328:391–407
- Ross NL and Hazen RM (1989) Single Crystal X-ray diffraction study of MgSiO₃ perovskite from 77 to 400 K. *Phys. Chem. Miner.* 16:415–420
- Sekiguchi S, Fujimoto M, Kang MG, Koizumi S, Cho SB and Tanaka J (1998) Structure analysis of SrTiO₃ (111) polar surfaces. *Jpn. J. Appl. Phys.* 37:4140–4143
- Sigmund WM, Rotov M, Jiang QD, Brunen J, Zegenhagen J and Aldinger F (1997) A titanium-rich (111) surface of SrTiO₃ single crystals by thermal annealing. *Appl. Phys. A* 64:219–220
- Stixrude L, Cohen RE, Hemley RJ (1998) Theory of minerals at high pressure. *Rev. Mineral* 37:639–671
- Stixrude L and Cohen RE (1993) Stability of orthorhombic MgSiO₃ perovskite in the earth's lower mantle. *Nature* 364:613–616
- Tanaka H and Kawai T (1996) Surface structure of reduced SrTiO₃(111) observed by scanning tunneling microscopy. *Surf. Sci.* 365:437–442
- Tasker PW (1979) The stability of ionic crystal surfaces. *J. Phys. C: Solid State Phys.* 12:4977–4984
- Urusov VS (1975) *Energetic Crystal Chemistry*, Nuka, Moscow; 335 (in Russian)
- Vanderbilt D (1990) Soft self-consistent pseudopotentials in a generalised eigenvalue formalism. *Phys. Rev. B.* 41:7892–7895
- Wall A and Price GD (1989) Electrical-conductivity of the lower mantle – a molecular-dynamics simulation of MgSiO₃ perovskite. *Phys. of Earth and Planet. In.* 58:192–204
- Wall A, Price GD and Parker SC (1986), A computer-simulation of the structure and elastic properties of MgSiO₃ perovskite. *Mineral. Magaz.* 50:693–707
- Wang ZC, Mei S, Karato S and Wirth R (1999) Grain growth in CaTiO₃-perovskite + FeO-wüstite aggregates. *Phys. Chem. Miner.* 27:11–19
- Watson GW, Wall A and Parker SC (2000) Atomistic simulation of the effect of temperature and pressure on point defect formation in MgSiO₃ perovskite and the stability of CaSiO₃ perovskite. *J. of Physics-Condensed Matter* 12:8427–8438
- Wright K and Price GD (1993) Computer-simulation of defects and diffusion in perovskites. *J. of Geophys. Research-solid Earth* 98(B12): 22245–22253
- Wright K and Price GD (1989) Computer-simulations of iron in magnesium-silicate perovskite. *Geophys. Reserch Lett.* 16:1399–1402
- Wyckoff RWG (1965) *Crystal Structures* volume 1, 2nd ed., John Wiley and Sons, New York, US
- Yamazaki D, Kato T, Yurimoto H, Ohtani E and Toriumi M (2000) Silicon self-diffusion in MgSiO₃ perovskite at 25 GPa. *Phys. Earth Planet. Int.* 119:299–309
- Yeganeh-Haeri A (1994) Synthesis and re-investigation of the elastic properties of single-crystal magnesium silicate perovskite. *Phys. Earth Planet. Inter.* 87:111–121